Journal of Molecular Catalysis A: Chemical 312 (2009) 53–64

Contents lists available at ScienceDirect

Journal of Molecular Catalysis A: Chemical

journal homepage: www.elsevier.com/locate/molcata

Designing heterogeneous oxovanadium and copper acetylacetonate catalysts: Effect of covalent immobilisation in epoxidation and aziridination reactions

Clara Pereira [a], Krzysztof Biernacki [a], Susana L.H. Rebelo [a], Alexandre L. Magalhães [a], Ana Paula Carvalho [b], João Pires [b,*], Cristina Freire [a,**]

[a] *REQUIMTE, Departamento de Química, Faculdade de Ciências, Universidade do Porto, R. Campo Alegre, 4169-007 Porto, Portugal*
[b] *Departamento de Química e Bioquímica, Centro de Química e Bioquímica, Faculdade de Ciências, Universidade de Lisboa, Campo Grande Ed. C8, 1749-016 Lisboa, Portugal*

ARTICLE INFO

Article history:
Received 26 January 2009
Received in revised form 30 June 2009
Accepted 3 July 2009
Available online 3 August 2009

Keywords:
Acetylacetonate complexes
Porous clay heterostructure
SBA-15
Allylic epoxidation
Olefin aziridination

ABSTRACT

Oxovanadium(IV) and copper(II) acetylacetonate complexes were immobilised onto a porous clay heterostructure (PCH) and SBA-15 previously functionalised with 3-aminopropyltriethoxysilane (APTES). The materials were characterised by chemical analysis, nitrogen adsorption–desorption isotherms at −196 °C, powder X-ray diffraction, X-ray photoelectron spectroscopy and Fourier transform infrared spectroscopy. The results indicated that APTES was grafted onto PCH and SBA-15 with 75% and 67% of efficiencies, respectively. Both complexes were successfully anchored onto the APTES-functionalised supports, although with different immobilisation efficiencies: [VO(acac)$_2$] was anchored with 57% and 91% of efficiencies onto PCH and SBA-15, respectively, whereas [Cu(acac)$_2$] was immobilised onto PCH and SBA-15 with 31% and 95% of efficiencies, respectively.

The [VO(acac)$_2$] heterogeneous materials acted as active catalysts in the epoxidation of geraniol using *tert*-butyl hydroperoxide as oxidant, presenting moderate substrate conversions, high selectivities towards 2,3-epoxygeraniol and very high stabilities upon reuse for two cycles. The [Cu(acac)$_2$] based materials were tested in the aziridination of styrene using [*N*-(*p*-tolylsulfonyl)imino]phenyliodinane as nitrogen source, showing moderate substrate conversions, but with considerable complex leaching after three cycles, indicating that the complex grafting methodology was not stable under aziridination catalytic conditions. Generically, the PCH based catalysts, although presenting lower metal contents, acted as more active and robust catalysts in the reactions tested.

1. Introduction

The catalytic synthesis of epoxides and aziridines is a theme of considerable interest since these products are valuable intermediates in organic synthesis [1–6]. Oxovanadium(IV) acetylacetonate ([VO(acac)$_2$]) is a very efficient homogeneous catalyst in the epoxidation of allylic alcohols using *tert*-butyl hydroperoxide (*t*-BuOOH) as oxidant, presenting high activity, stereo- and regioselectivity [1,7–9]. On the other hand, copper(II) acetylacetonate ([Cu(acac)$_2$]) has also been reported as a very effective homogeneous catalyst in the aziridination of alkenes using [*N*-(*p*-tolylsulfonyl)imino]phenyliodinane (PhI = NTs) as nitrogen source [3].

Despite the advantages inherent to homogeneous catalysts, the problems associated with the catalysts separation and recycling from the reaction media as well as their low chemical and thermal stability are major drawbacks towards a sustainable chemistry [10–13]. One of the possible approaches to overcome these problems is their immobilisation onto solid supports that can be either inorganic materials or organic polymers [10–13].

Several studies regarding the immobilisation of [VO(acac)$_2$] and [Cu(acac)$_2$] complexes onto solid supports for subsequent application in the epoxidation of allylic alcohols and in the aziridination of olefins, respectively, have been reported in literature [5,6,14–17]. These complexes have already been immobilised in smectite-type clays either directly or after their functionalisation with amine groups [14,18], in amine-functionalised activated carbons [15,16,19] and mesoporous silicas [17] and in polystyrene by microencapsulation [5,6]. These complexes have also been directly anchored onto alumina, silica gel and mesoporous silicas (MCM, SBA, MCF and MSU) with subsequent calcination to produce metal dispersed catalysts [20–23]. According to literature, the direct grafting of [M(acac)$_2$] complexes occurs by the reaction between the complex and the free silanol groups of the support, following one of two possible mechanisms: (i) hydrogen bonding mechanism between the

* Corresponding author. Tel.: +351 21 7500898; fax: +351 21 7500088.
** Corresponding author. Tel.: +351 22 0402590; fax: +351 22 0402659.
E-mail addresses: jpsilva@fc.ul.pt (J. Pires), acfreire@fc.up.pt (C. Freire).

1381-1169/$ – see front matter © 2009 Elsevier B.V. All rights reserved.
doi:10.1016/j.molcata.2009.07.004

pseudo π system of the acetylacetonate (acac) ligand and the silanol protons of the support or (ii) by a ligand-exchange mechanism with the formation of a covalent bond between the metal centre and an oxygen atom of the support [14,18,20–23]. In the case of amine-functionalised supports, the metal complexes are anchored by Schiff base condensation between the carbonyl group of the acac ligand and the free amine groups previously grafted onto the materials surface [14–19]. The microencapsulation within polymers, on the other hand, consists in the physical envelopment of the complexes by a thin polymer film involving interactions between the π electrons of the polymer benzene rings and the complex vacant orbitals [5,6].

In terms of catalytic performance, the [VO(acac)$_2$] based materials prepared by microencapsulation in polystyrene [5] and by immobilisation in amine-functionalised activated carbon [15] and K10-montmorillonite clay [14] presented similar catalytic activities in the epoxidation of allylic alcohols as the homogeneous counterpart and good/moderate stabilities upon reuse in further catalytic cycles. The [Cu(acac)$_2$] complex microencapsulated in polystyrene [6] and immobilised onto amine-functionalised activated carbon [16] and mesoporous silica [17] acted as recyclable and reusable catalysts in the aziridination of olefins, with similar catalytic activities as the homogeneous analogue.

The quest for novel supporting materials for the immobilisation of these complexes has been the focus of continuous research with the aim of designing new heterogeneous catalysts that combine the advantages of homogeneous and heterogeneous catalysis. In this way, new insights regarding the immobilisation mechanisms as well as the influence of the supports themselves (structure, composition and porosity) in the anchoring efficiencies and catalytic activities have to be achieved.

Porous clays heterostructures (PCHs) are a relatively new class of porous materials mainly composed of lamellar clay frameworks and silica pillars within the interlayers spaces, with pore sizes in the supermicropore to small mesopore region and high specific surface areas in the range of 700–1000 m^2 g^{-1} [24,25]. Due to their larger pore sizes and higher surface areas, PCHs overcome some limitations inherent to clays and to traditional pillared clays (PILCs). In recent years several properties of PCHs have been studied [26,27], including their performance as catalysts [24] and as adsorbents [28,29].

SBA-15, is a mesoporous silica with a highly ordered hexagonal structure, high surface area and uniform pores size distribution ranging from 5 to 30 nm, prepared from an amphiphilic triblock copolymer [30,31]. It presents more uniform porosity than PCH, but when properties such as thermal and hydrothermal stabilities are compared, PCHs are more stable than SBA-15 based materials [32,33]. SBA-15 has already been studied as catalysts support, although in a reduced number of publications [34,35].

In the present work [VO(acac)$_2$] and [Cu(acac)$_2$] were immobilised onto the porous materials PCH and SBA-15 previously functionalised with APTES. The catalytic activities of the anchored [VO(acac)$_2$] and [Cu(acac)$_2$] complexes were studied, at room temperature, in the epoxidation of geraniol using *t*-BuOOH as oxidant and in the aziridination of styrene using PhI = NTs as nitrogen source, respectively, and compared with the performance of the corresponding homogeneous catalysts. The aim of this work is to investigate the effect of the support structure/porosity in the immobilisation efficiencies and location of the grafted complexes. Furthermore, we examine the influence of covalent grafting on the catalysts performance and stability, to provide new insights regarding the differences between heterogeneous and homogeneous catalytic reactions. To the best of our knowledge this is the first work where a PCH is considered as support of transition metal complexes and compared with a mesoporous silica analogue.

2. Experimental

2.1. Reagents and solvents

[VO(acac)$_2$], [Cu(acac)$_2$], APTES, styrene, chlorobenzene, geraniol, *t*-BuOOH solution 5.0–6.0 M in decane, dry toluene, cetyltrimethylammonium bromide (CTAB), dodecylamine, tetraethylorthosilicate (TEOS) and poly(ethylene glycol)-*block*-poly(propylene glycol)-*block*-poly(ethylene glycol) (Pluronic P123, M_n ~5.800) were purchased from Aldrich. The solvents CH_3CN and CH_2Cl_2 were supplied by Romil (HPLC grade) and $CHCl_3$ was from Merck. Silica gel 60 and TLC plastic sheets of silica gel 60 F_{254} were from Merck.

2.2. Catalysts preparation

2.2.1. Synthesis of PCH

PCH was synthesised after optimisation of procedures described in literature [25,27]. A suspension of a Portuguese montmorillonite clay (1 g in 100 cm^3 of water) was firstly equilibrated with a 0.5 M solution of CTAB, under stirring at 50 °C overnight. The solid was then separated from solution, washed until pH 7 was reached and air-dried. To the resulting solid a given amount of dodecylamine was added under stirring, and after 20 min, TEOS was added as the silica source. After mixing for 3 h, the solid was air-dried and calcined at 650 °C for 5 h with a ramp of 1 °C min^{-1}.

2.2.2. Synthesis of SBA-15

SBA-15 was obtained following a procedure adapted from literature [30]. An aqueous solution of HCl (1.6 M) was added dropwise to a triblock copolymer surfactant (Pluronic P123) dissolved in water (8 g dm^{-3}); TEOS was then added dropwise and the mixture was stirred, put in an oven at 35 °C for 24 h and more 24 h at 100 °C. The solid was filtered and calcined at 550 °C for 5 h with a ramp of 1 °C min^{-1}.

2.2.3. Functionalisation of PCH and SBA-15 with APTES

The parent materials (PCH or SBA-15) were dried in an oven at 120 °C for 1 h, under vacuum, to remove any physisorbed water. Afterwards, a mixture of 2.00 g of material in 100 cm^3 of dry toluene and 1.18 cm^3 of APTES (5.06 mmol) was refluxed for 24 h under argon atmosphere. The resulting materials (APTES@PCH or APTES@SBA-15) were then vacuum-filtered, refluxed with 100 cm^3 of dry toluene for 2 h and dried under vacuum at 120 °C for 3 h.

2.2.4. Anchoring of [M(acac)$_2$] complexes (M = VO(IV) or Cu(II)) onto APTES-functionalised materials

A solution of 90 μmol of [M(acac)$_2$] in 50 cm^3 of $CHCl_3$ was refluxed with 0.60 g of APTES-functionalised material for 24 h. The resulting materials were vacuum-filtered, refluxed with 50 cm^3 of $CHCl_3$ for 2 h and then dried under vacuum at 120 °C for 3 h. The materials will be referred to as [VO(acac)$_2$]APTES@PCH, [VO(acac)$_2$]APTES@SBA-15, [Cu(acac)$_2$]APTES@PCH and [Cu(acac)$_2$]APTES@SBA-15.

The summary of all the steps followed in the immobilisation of [VO(acac)$_2$] and [Cu(acac)$_2$] in both materials is presented in Scheme 1.

2.3. Physico-chemical characterisation

Nitrogen adsorption–desorption isotherms at −196 °C were measured in an automatic apparatus (Asap 2010; Micromeritics). Before the adsorption experiments the samples were outgassed under vacuum during 2.5 h at 150 °C. The specific surface areas were calculated from the BET model [36] and the porous volumes

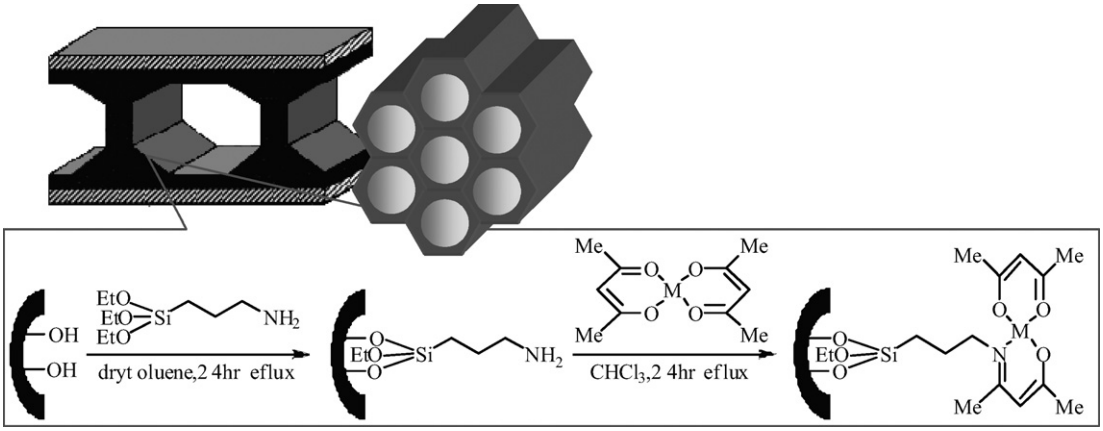

Scheme 1. Schematic representation of [M(acac)$_2$] (M = VO(IV) or Cu(II)) complexes immobilisation onto APTES-functionalised porous silica supports.

were estimated from the α_s-method, using a dehydroxylated silica as reference material [36].

Powder X-ray diffraction (PXRD) patterns of SBA-15 and functionalised materials were obtained on a Philips Analytical PW 3050/60 X'Pert PRO(theta/2theta) with automatic data acquisition (X'Pert Data Collector (v2.0b) software), using a monochromatised CuKα radiation as incident beam. Diffractograms were obtained by continuous scanning from 0.8 to 2.5° 2θ, with a step size of 0.03° 2θ and a time per step of 40 s.

Vanadium contents obtained by inductively coupled plasma emission spectrometry (ICP-AES) and nitrogen elemental analysis (EA) were performed at "Laboratório de Análises", IST, Lisboa (Portugal). The copper contents were determined by atomic absorption spectroscopy (AAS) in a Pye Unicam SP9 spectrometer. Samples (20 mg) were previously dried at 100 °C, mixed with 2 cm^3 of *aqua regia* and 3 cm^3 of HF for 2 h at 120 °C, in a stainless steel autoclave equipped with a polyethylene-covered beaker (ILC B240).

X-ray photoelectron spectroscopy (XPS) was performed at "Centro de Materiais da Universidade do Porto" (Portugal), in a VG Scientific ESCALAB 200A spectrometer using non-monochromatised Al Kα radiation (1486.6 eV). The materials were compressed into pellets prior to the XPS studies. To correct possible deviations caused by electric charge of the samples, the C 1s band at 285.0 eV was taken as internal standard. The XPS spectra were deconvoluted with the XPSPEAK 4.1 software, using non-linear least squares fitting routine after a Shirley-type background subtraction. The surface atomic percentages were calculated from the corresponding peak areas and using the sensitivity factors provided by the manufacturer.

The Fourier transform infrared (FTIR) spectra of the compounds were collected with a Jasco FT/IR-460 Plus spectrophotometer in the 400–4000 cm^{-1} range, using a resolution of 4 cm^{-1} and 32 scans. The spectra of the samples were obtained in KBr pellets (Merck, spectroscopic grade) containing 0.4 wt% of material. All samples and KBr were dried at 100 °C overnight before KBr pellets preparation.

The ^{1}H NMR spectra were recorded using a Bruker DRX 300 at 300.13 MHz and TMS as the internal standard.

GC-FID chromatograms were obtained with a Varian CP-3380 gas chromatograph equipped with a FID detector, using helium as carrier gas and a fused silica Varian Chrompack capillary column CP-Sil 8 CB Low Bleed/MS (30 m × 0.25 mm i.d.; 0.25 μm film thickness). Temperature program for geraniol epoxidation reactions: 40 °C (1 min), 25 °C min^{-1}, 150 °C, 5 °C min^{-1}, 200 °C (1 min); injector temperature, 200 °C; detector temperature, 250 °C. Conditions for styrene aziridination reactions: 70 °C (1 min), 8 °C min^{-1}, 150 °C (0.5 min), 28°C min^{-1}, 200 °C (0.5 min); injector temperature, 200 °C; detector temperature, 230 °C.

GC–MS analyses were performed with a Finnigan Trace GC–MS (Thermo Quest CE Instruments) using helium as the carrier gas (35 cm s^{-1}) equipped with a SPB-5 capillary column (30 m × 0.25 mm i.d.; 0.25 μm film thickness). Temperature program for epoxidation reaction mixtures: 80 °C (1 min), 25 °C min^{-1}, 155 °C, 5 °C min^{-1}, 200 °C; injector temperature, 220 °C; interface and oven temperatures, 280 °C.

2.4. Computational details

The structure of the [VO(acac)$_2$]-APTES molecule was obtained by complete optimisation in vacuum without any geometrical constraints using the B3-LYP hybrid functional within the density functional theory (DFT) [37,38]. The double-zeta Pople basis set 6–31G (d,p) was used for all the atoms except vanadium, for which the LANL2DZ effective core potential was applied [39]. The optimised structure was used to calculate the fundamental IR vibrational frequencies at the same DFT level, which is still one of the recommended theoretical methods for IR spectra prediction according to a recent study of Merrick et al. [40]. All *ab initio* calculations were performed with Gaussian03 program package [41] and the visualisation of the normal vibration modes was possible by means of GaussView4.1 [42].

It is well known that, in general, *ab initio* harmonic frequencies are overestimated when compared with the experimental values. In a recent work carried out with a long list of theory levels and a set of more than one thousand normal vibration modes, the optimal value $\lambda = 0.9627$ was proposed as the scale factor to be used at the B3LYP/6-31G (d,p) level [40]. However, this type of scale factors is based on a very heterogeneous sample of vibration modes, and thus the success of the application to a particular molecular system is not guaranteed. In this context, we decided to find a scaling procedure especially devised to the [VO(acac)$_2$]-APTES molecule. We calculated the harmonic frequencies of the parent complex [VO(acac)$_2$] at the same level of theory, and performed a linear least squares fitting with the available experimental data in the 1000–1600 cm^{-1} range [43]. Six particular frequencies (997, 1287, 1371, 1523, 1547 and 1561 cm^{-1}) were chosen in the IR spectrum region, for which there were no ambiguities about the assignments. The linear relationship $\upsilon_{corr} = 1.120\upsilon_{exp} - 218$ was obtained with a reasonable linear regression coefficient $r^2 = 0.9966$.

2.5. Catalytic studies

The [VO(acac)$_2$] and [Cu(acac)$_2$] heterogeneous materials were tested as catalysts in the geraniol epoxidation and styrene aziridination, respectively. The catalytic reactions were also performed

under similar conditions in (a) homogeneous phase using the same [M(acac)$_2$] contents as those of the heterogeneous materials, and (b) using the parent and APTES-functionalised supports without any added complex.

To monitor the reaction progress, 0.05 cm^3 aliquots were withdrawn from the reaction mixture with a hypodermic syringe, filtered through 0.2 μm PTFE syringe filters and directly analysed by GC.

2.5.1. Epoxidation of geraniol

In a typical procedure, 1.00 mmol of geraniol 0.50 mmol of chlorobenzene (internal standard) and 0.10 g of [VO(acac)$_2$] based material were mixed in 5.00 cm^3 of CH_2Cl_2, at room temperature with continuous stirring. The *t*-BuOOH, 1.50 mmol, was progressively added to the reaction using a Bioblock Scientific Syringe Pump at a rate of 3.05 cm^3 h^{-1}. At the end, the heterogeneous catalyst was filtered and then refluxed/filtered with 50 cm^3 of CH_2Cl_2 for 2 h, dried under vacuum at 120 °C during 2 h, and reused two times.

The ^{1}H NMR spectra of the reaction mixtures were obtained in $CDCl_3$ and the substrate conversions and products yields were calculated based on the integration of chosen proton signals (δ(ppm) = 5.08 for 2,3-epoxygeraniol and δ(ppm) = 5.10 and 5.40 for geraniol).

At the end of the homogeneous reactions the products were isolated by silica gel column chromatography using a mixture of CH_2Cl_2:ethyl acetate (9:1) as eluent, affording 2,3-epoxygeraniol in a 92% yield. The chromatography was controlled by TLC on silica sheets and the spots were visualised by treatment with a mixture of sulphuric acid:methanol (1:1).

2.5.1.1. 2,3-Epoxygeraniol. ^{1}H NMR (300 MHz, $CDCl_3$, 22 °C, TMS): δ(ppm) = 1.29 (s, 3H, H-10), 1.22–1.26 and 1.45–1.49 (2m, 2H, H-5), 1.61 (s, 3H, H-8), 1.68 (d, *J* = 0.9 Hz, 3H, H-9), 2.04–2.12 (m, 2H, H-4), 2.98 (dd, *J* = 4.1 and 6.8 Hz, 1H, H-2), 3.49 (s-broad, 1H, OH), 3.65 (dd, *J* = 6.8 and 12.2 Hz, 1H, H-1), 3.81 (dd, *J* = 4.1 and 12.2 Hz, 1H, H-1), 5.08 (tt, *J* = 1.3 and 7.1 Hz, 1H, H-6). MS (70 eV, EI): *m*/*z* (%): 170 (1) [$M^{+\bullet}$], 152 (4), 139 (8), 137 (5), 121 (13), 109 (100).

2.5.2. Aziridination of styrene

The styrene aziridination was carried out at room temperature using 1.22 mmol of styrene, 1.22 mmol of chlorobenzene, 0.10 g of [Cu(acac)$_2$] based material and 0.244 mmol of PhI = NTs in 5.00 cm^3 of CH_3CN, under stirring conditions. After reaction, the catalyst was removed by filtration, refluxed/filtered sequentially with 50 cm^3 of methanol for 2 h and with 50 cm^3 of CH_3CN for 2 h, dried under vacuum at 120 °C during 2 h, and reused two times.

The PhI = NTS was synthesised according to procedures described in the literature [44], in a 75% yield. ^{1}H NMR (300 MHz, $CDCl_3$, 22 °C, TMS): δ(ppm) = 2.44 (s, 3H, CH_3), 7.11 (t, *J* = 7.8 Hz, 2H, H-Ar), 7.31–7.36 (m, 3H, H-Ar), 7.70 (dd, *J* = 8.2 and 1.0 Hz, 2H, H-Ar), 7.82 (d, *J* = 8.2 Hz, 2H, H-Ar).

At the end of the homogeneous reactions the products were isolated by column chromatography on silica gel using a mixture of *n*-hexane:ethyl acetate (6:1) as eluent. Instead of column chromatographic separation, the reaction mixture can be passed through a small plug of silica and eluted with CH_2Cl_2, followed by solvent evaporation under reduced pressure, treatment with CH_2Cl_2:petroleum ether and subsequent filtration to remove the precipitated *p*-toluenesulfonamide.

2.5.2.1. N-(p-tolylsulfonyl)-2-phenylaziridine. ^{1}H NMR (300 MHz, $CDCl_3$, 22 °C, TMS): δ(ppm) = 2.39 (d, *J* = 4.4 Hz, 1H, H-3*trans*), 2.43 (s, 3H, CH_3), 2.98 (d, *J* = 7.2 Hz, 1H, H-3*cis*), 3.78 (dd, *J* = 4.4 and 7.2 Hz, 1H, H-2), 7.20–7.34 (m, 7H, H-Ar), 7.87 (d, *J* = 8.3 Hz, 2H, H-Ar).

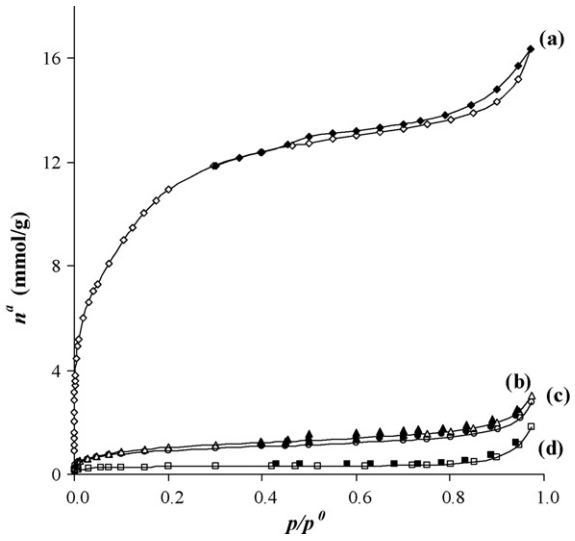

Fig. 1. Nitrogen adsorption–desorption isotherms for PCH based materials: (a) PCH, (b) APTES@PCH, (c) [Cu(acac)$_2$]APTES@PCH and (d) [VO(acac)$_2$]APTES@PCH. Open points for adsorption and closed points for desorption.

2.5.2.2. p-Toluenesulfonamide. ^{1}H NMR (300 MHz, $CDCl_3$, 22 °C, TMS): δ(ppm) = 2.44 (s, 3H, CH_3), 4.73 (s-broad, 2H, NH_2), 7.32 (d, *J* = 8.3 Hz, 2H, H-Ar), 7.82 (d, *J* = 8.3 Hz, 2H, H-Ar).

3. Results and discussion

3.1. Chemical and textural characterisation

The nitrogen adsorption–desorption isotherms at −196 °C are presented in Figs. 1 and 2 for the PCH and SBA-15 based materials, respectively. In the case of the PCH starting material, the shape of the isotherm has a very open "knee" (Fig. 1), being in accordance with the results reported in literature for this type of materials [25,45] and consistent with a material with small size mesopores. The PCH has maxima values at 2.1 and 2.6 nm in the mesopores size distribution. For SBA-15, the isotherm has its characteristic shape (Fig. 2(A)) [46], with a hysteresis cycle typical of type IV isotherms [36]. In terms of mesopores size distribution (Fig. 2(B)) obtained from the BdB–FHH method [47], the pores widths of the initial SBA-15 are centred at 6.4 nm and the pores size distribution is narrow as expected for this type of material with uniform porosity.

Upon functionalisation with APTES, a drastic decrease in the pore volumes is noticed for PCH and SBA-15 (Table 1). In fact, in both materials the absolute value of the decrease is similar (0.35–0.40 cm^3 g^{-1}) but the consequences are more drastic for the PCH due to its lower initial pore volume (Figs. 1 and 2, Table 1). While APTES@SBA-15 still retains characteristics of a mesoporous material, the APTES@PCH sample is essentially nonporous as denoted by the low values of the specific surface and confirmed from the analysis by the α_s-method [36]. These observations can apply to the final materials after the immobilisation of the [M(acac)$_2$] complexes. In the case of SBA-15, the mesopores size is only slightly shifted to a lower value upon funtionalisation with APTES and complexes anchoring, that is, a reduction from 6.4 nm in the initial sample to, in average, 5.6 nm in the remaining materials (Fig. 2(B)). In the case of PCH, for the reasons already mentioned, only for the initial sample a reliable pores size distribution could be obtained. As discussed in more detail below, these marked differences between the textural properties of PCH and SBA-15 based materials are not directly reflected in the respective catalytic properties.

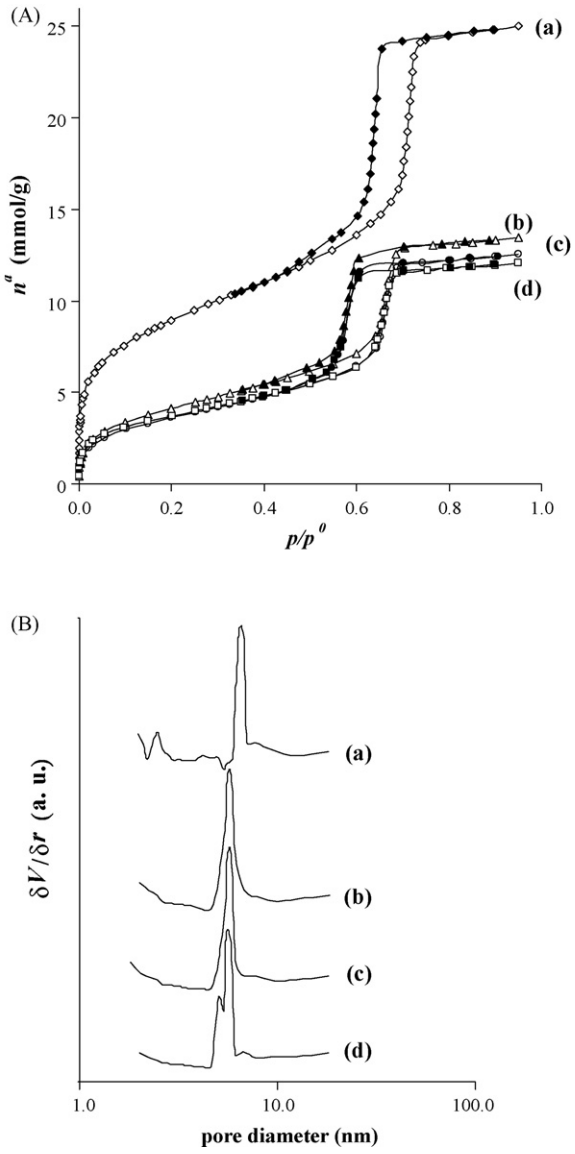

Fig. 2. Nitrogen adsorption–desorption isotherms at −196 °C (A) and mesopores size distributions (B) for SBA-15 based materials: (a) SBA-15, (b) APTES@SBA-15, (c) [VO(acac)$_2$]APTES@SBA-15 and (d) [Cu(acac)$_2$]APTES@SBA-15. Open points for adsorption and closed points for desorption.

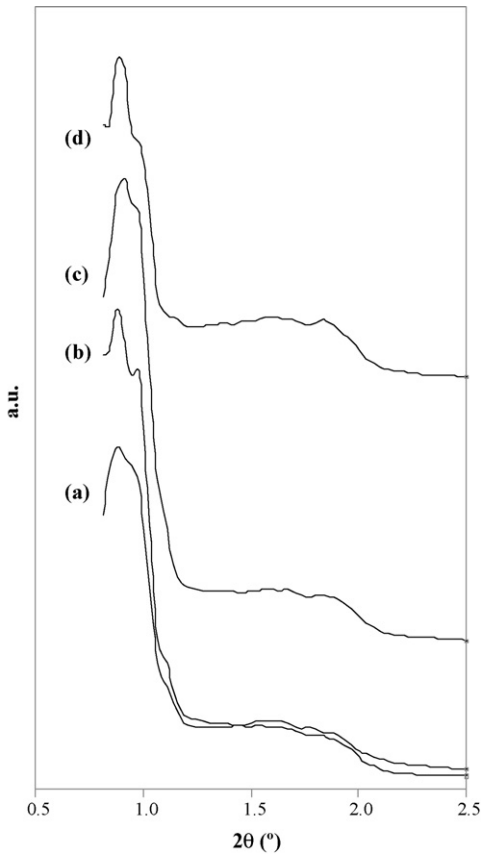

Fig. 3. Low-angle X-ray diffraction patterns of (a) SBA-15, (b) APTES@SBA-15, (c) [VO(acac)$_2$]APTES@SBA-15 and (d) [Cu(acac)$_2$]APTES@SBA-15.

The low-angle PXRD patterns of the SBA-15 based materials (Fig. 3) show that neither the funtionalisation nor the posterior anchorage of the metallic complexes result in structural alterations, since in all cases the d_{100} diffraction peak appears at the expected value [30].

To ascertain the APTES and [M(acac)$_2$] grafting efficiencies, the nitrogen and metal bulk contents were determined (Table 1). The N bulk contents indicate that APTES was grafted onto both PCH and SBA-15 materials, with efficiencies (amount of grafted APTES/amount used in the functionalisation reaction × 100) of 75% and 67%, respectively.

The [VO(acac)$_2$] complex was immobilised with anchoring efficiencies (amount of anchored complex/amount in original solution × 100) of 57% and 91% for [VO(acac)$_2$]APTES@PCH and [VO(acac)$_2$]APTES@SBA-15, respectively. The same pattern is also

Table 1
Chemical and textural properties of silica based materials.

Material	N (mmol g^{-1})		V (μmol g^{-1})		Cu (μmol g^{-1})		Textural properties	
	EA	XPS[a]	ICP	XPS[a]	AAS	XPS[a]	A_{BET} (m^2 g^{-1})	$V_{micro+meso}$[b] (cm^3 g^{-1})
PCH	–	–	–	–	–	–	908	0.45
APTES@PCH	1.9	ND	–	–	–	–	85	–
[VO(acac)$_2$]APTES@PCH	1.9	1.6	86	107	–	–	50	–
[Cu(acac)$_2$]APTES@PCH	1.8	1.6	–	–	47	87	75	–
SBA-15	–	–	–	–	–	–	728	0.81
APTES@SBA-15	1.7	1.5	–	–	–	–	344	0.46
[VO(acac)$_2$]APTES@SBA-15	1.6	1.2	137	53	–	–	300	0.42
[Cu(acac)$_2$]APTES@SBA-15	1.4	1.3	–	–	142	213	302	0.41

[a] Surface contents determined from XPS data in Table 2: mmol N/weight of material = atomic % N/Σ[atomic % (i) × Ar(i)]; μmol V/weight of material = atomic % V/Σ[atomic % (i) × Ar(i)]; μmol Cu/weight of material = atomic % Cu/Σ[atomic % (i) × Ar(i)].

[b] Microporous plus mesoporous volume determined by the α_s-method.

Table 2
XPS atomic percentages for silica based materials[a].

Material	Atomic %								
	C 1s	O 1s	N 1s	Mg 1s	Si 2p	Al 2p	Fe $2p_{3/2}$	Cu $2p_{3/2}$	V[b] $2p_{3/2}$
PCH	6.33	60.94	0.66	0.41	30.09	1.04	0.54	–	–
[$VO(acac)_2$]APTES@PCH	18.70	50.72	2.98	0.23	26.52	0.36	0.27	–	0.2
[$Cu(acac)_2$]APTES@PCH	17.84	51.39	3.07	0.27	27.03	ND[c]	0.24	0.16	–
SBA-15	2.86	63.10	0.17	–	33.87	–	–	–	–
APTES@SBA-15	15.80	51.72	2.76	–	29.71	–	–	–	–
[$VO(acac)_2$]APTES@SBA-15	14.81	53.69	2.27	–	29.14	–	–	–	0.1
[$Cu(acac)_2$]APTES@SBA-15	13.35	54.08	2.49	–	29.67	–	–	0.41	–

[a] Determined by the area of the respective bands in the high resolution XPS spectra.
[b] Estimated by modulation of the band which includes two O 1s satellite peaks.
[c] Not determined due to overlapping between the Al 2p and Cu ($3p_{3/2}$; $3p_{1/2}$) peaks.

observed in the case of [$Cu(acac)_2$] immobilisation, which led to anchoring efficiencies of 31% and 95% for [$Cu(acac)_2$]APTES@PCH and [$Cu(acac)_2$]APTES@SBA-15, respectively. However, if the anchoring efficiencies are calculated based on the grafted APTES loadings, by assuming that the complexes are only immobilised through the grafted spacer, the anchoring efficiencies of metal complex towards the linker are only of 4% and 2% for [$VO(acac)_2$]APTES@PCH and [$Cu(acac)_2$]APTES@PCH and of 8% for both [$M(acac)_2$]APTES@SBA-15 materials. These facts suggest that a significant amount of free amine groups remains on the materials surfaces after the complexes immobilisation. Additionally, although both APTES-functionalised materials present almost the same N content, the APTES@SBA-15 support anchors higher quantities of metal complexes.

The eventual APTES leaching during the complexes grafting was checked by N bulk contents: in [$M(acac)_2$]APTES@PCH materials and [$VO(acac)_2$]APTES@SBA-15 they are identical to those of the amine-functionalised supports, but in [$Cu(acac)_2$]APTES@SBA-15 the value is slightly lower probably due to some leaching of APTES.

The surface atomic contents and the core level binding energies (BEs), determined by XPS (Tables 2 and 3), provide insights concerning the materials chemical composition/structure and the grafting reaction mechanisms.

PCH and SBA-15 are mainly composed of O and Si, in a Si/O ratio consistent with the expected SiO_2 stoichiometry. The high-resolution XPS spectra exhibit the typical bands in the O 1s and Si 2p regions, centred at about 533.0–533.2 and 103.7–103.9 eV, respectively. The PCH material also presents small quantities of Al, Fe and Mg which are related with the clay framework and in accordance with its chemical composition [48]. The presence of small C and N contents is most probably related with some organic impurities from the materials synthesis.

In the case of APTES-modified materials, only APTES@SBA-15 was characterised by XPS, due to the scarce amount of APTES@PCH. The APTES functionalisation induces significant increases in the C and N contents and small decreases in the O and Si ones. The peaks in the O 1s and Si 2p regions are shifted to lower BEs and a new peak around 399.5 eV can be observed in the N 1s region, which corresponds to grafted amine groups [49–51]; the shoulder around 401.6 eV in the N 1s region may be due to some protonated amine species [49–51]. These facts confirm the APTES grafting by the reaction between the silica free silanol groups and the APTES ethoxyl functionalities. The comparison between the N bulk (EA) and surface (XPS) contents allows the location of APTES molecules within the materials. In APTES@SBA-15 the bulk N content is slightly higher than the surface one suggesting that the amine groups are almost homogeneously distributed throughout the support, although slightly more concentrated on the internal surface.

Upon anchoring of [$VO(acac)_2$] and [$Cu(acac)_2$] onto the APTES modified supports, the appearance of a new peak in the V $2p_{3/2}$ and Cu $2p_{3/2}$ regions, respectively, certifies the success of their immobilisation. When compared with the original samples,

Table 3
Core level binding energies of silica based materials obtained from curve fitting of the XPS spectra.

Material	BE (eV)[a]								
	C 1s	O 1s	N 1s	Mg 1s	Si 2p	Al 2p	Fe $2p_{3/2}$	Cu $2p_{3/2}$	V $2p_{3/2}$[b]
PCH	285.0 (2.5) 287.2 (3.0)	533.0 (2.6)	401.5 (4.3)	1304.3 (2.8)	103.7 (2.5)	75.0 (2.6)	711.2 (3.9)	–	–
[$VO(acac)_2$]APTES@PCH	285.0 (2.5) 287.0 (3.2)	532.6 (2.7)	399.9 (2.4) 401.8 (2.7)	1303.7 (2.6)	103.3 (2.6)	74.7 (2.9)	710.8 (4.7)	–	517.0 (3.0)
[$Cu(acac)_2$]APTES@PCH	285.0 (2.6) 287.3 (3.0)	532.7 (2.6)	400.0 (2.8) 402.1 (2.4)	1303.9 (2.7)	103.4 (2.6)	ND[c]	710.7 (4.1)	933.4 (2.8)	–
SBA-15	285.0 (2.5) 286.9 (3.0)	533.2 (2.6)	400.9 (4.9)	–	103.9 (2.6)	–	–	–	–
APTES@SBA-15	285.0 (2.6) 286.9 (2.7)	532.8 (2.8)	399.5 (2.5) 401.6 (2.4)	–	103.5 (2.8)	–	–	–	–
[$VO(acac)_2$]APTES@SBA-15	285.0 (2.6) 287.2 (3.0)	532.7 (2.8)	399.9 (3.0) 402.2 (2.9)	–	103.4 (2.7)	–	–	–	517.0 (3.0)
[$Cu(acac)_2$]APTES@SBA-15	285.0 (2.6) 287.3 (3.2)	532.8 (2.6)	400.0 (2.7) 402.0 (3.1)	–	103.5 (2.6)	–	–	933.3 (2.9)	–

[a] Values between brackets refer to the full-width at half maximum (FWHM) of the bands.
[b] Estimated by modulation of the band which includes two O 1s satellite peaks.
[c] Not determined due to overlapping between the Al 2p and Cu ($3p_{3/2}$; $3p_{1/2}$) peaks.

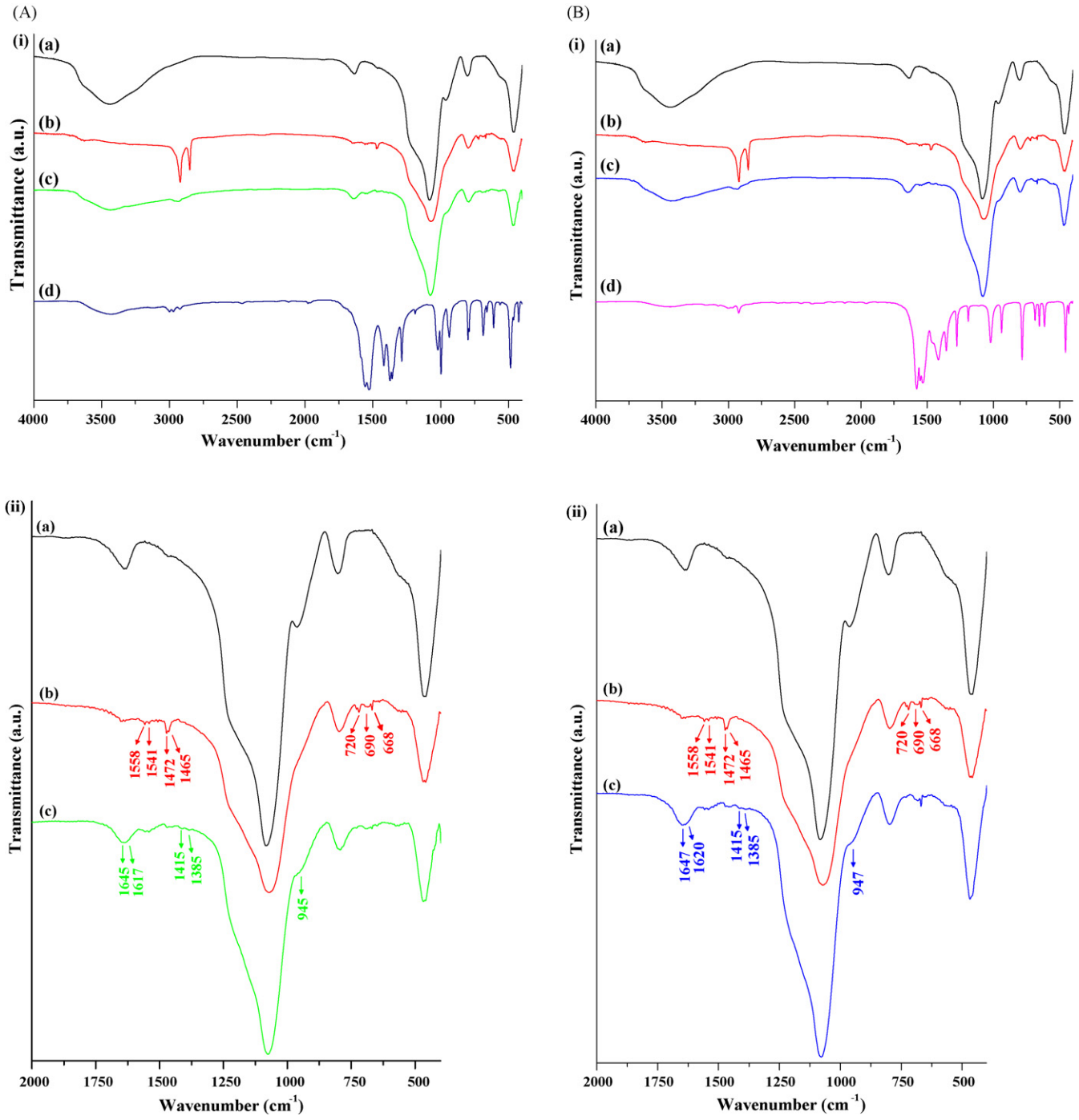

Fig. 4. FTIR spectra in the (i) 4000–400 cm^{-1} range and (ii) amplified 2000–400 cm^{-1} region of (A) [$VO(acac)_2$] PCH based materials (a) PCH, (b) APTES@PCH, (c) [$VO(acac)_2$]APTES@PCH and (d) [$VO(acac)_2$]; (B) [$Cu(acac)_2$] PCH based materials (a) PCH, (b) APTES@PCH, (c) [$Cu(acac)_2$]APTES@PCH and (d) [$Cu(acac)_2$].

[$M(acac)_2$]APTES@PCH materials present lower Mg, Fe and Al contents as well as small decreases in the respective core level BEs. However, no conclusions can be taken whether these changes are due to the complexes grafting or occur during the APTES functionalisation. In the case of SBA-15 materials, the [$M(acac)_2$] grafting does not introduce significant changes in the atomic percentages of the elements. However, the BEs of the N 1s peaks show small shifts to higher energies, suggesting a change in the nitrogen chemical environment.

The BEs of the V $2p_{3/2}$ and Cu $2p_{3/2}$ peaks in the free complexes were also determined (517.1 and 934.8 eV, respectively) and compared with those of the supported complexes. In both [$Cu(acac)_2$] based materials, the Cu $2p_{3/2}$ peak shows a shift of 1.5 eV to lower BEs, whereas in the [$VO(acac)_2$] based materials the BEs of the V $2p_{3/2}$ peak are almost the same as that of the free complex (0.1 eV shift). Nevertheless, in the latter case, the BEs can only be interpreted as a raw estimation, since V $2p_{3/2}$ peak is partially overlapped with the O 1s satellite peaks. These results are in accordance with those reported for the immobilisation of [$M(acac)_2$] complexes onto APTES-functionalised clays [18].

In [$VO(acac)_2$]APTES@PCH, [$Cu(acac)_2$]APTES@PCH and [$Cu(acac)_2$]APTES@SBA-15 the metal surface contents are higher than the bulk loadings, suggesting that the complexes are mostly immobilised onto the supports external surface. In contrast, in

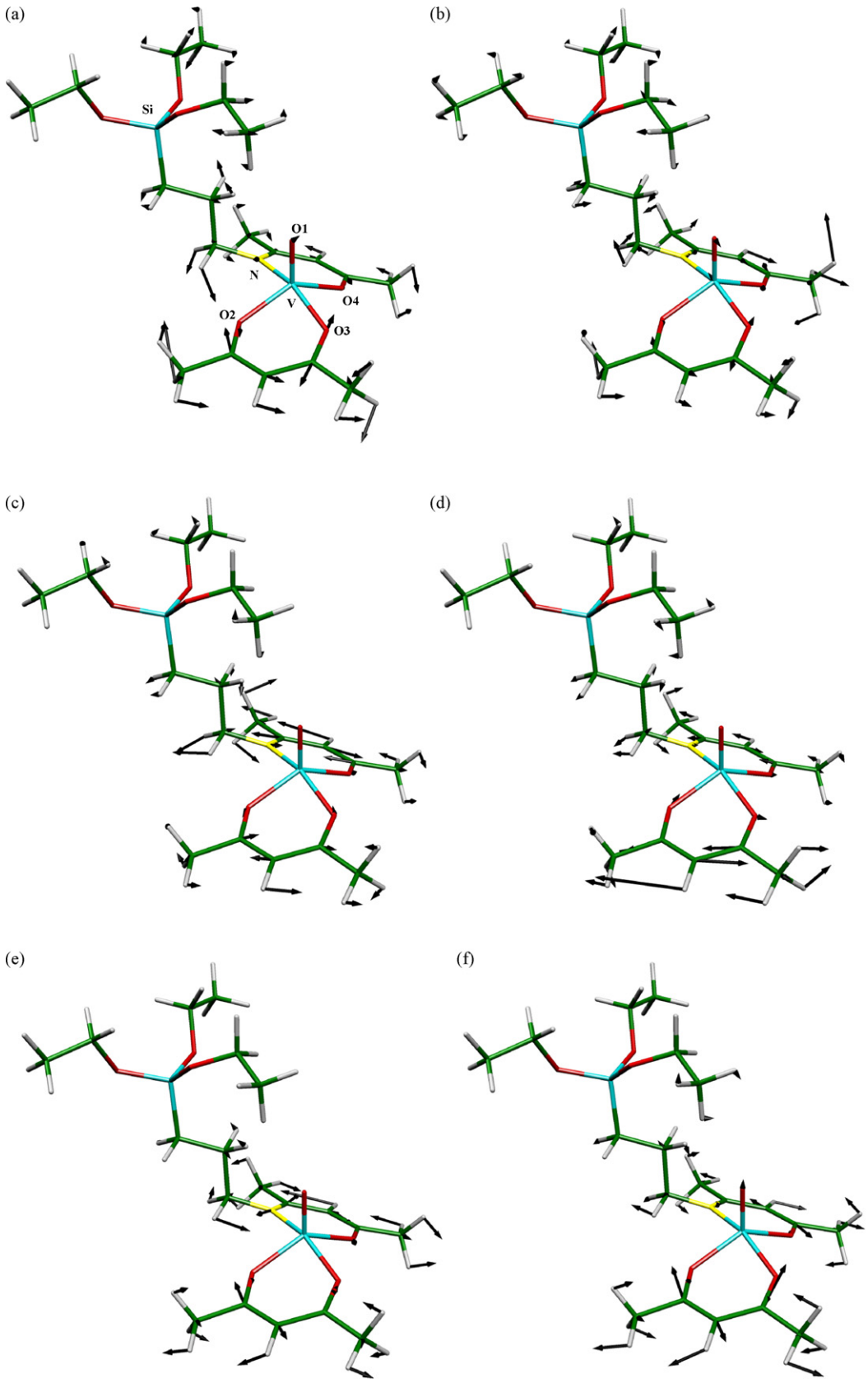

Fig. 5. Selected IR vibration modes, in the 1350–1700 cm^{-1} range, of the model molecule [$VO(acac)_2$]-APTES calculated at the DFT level (a) 1395 cm^{-1}, (b) 1418 cm^{-1}, (c) 1543 cm^{-1}, (d) 1545 cm^{-1}, (e) 1620 cm^{-1} and (f) 1634 cm^{-1}.

[VO(acac)$_2$]APTES@SBA-15, the complex is mainly anchored in the inner pores, since the V surface loading is lower than the bulk one.

3.2. FTIR studies

The FTIR spectra of PCH and SBA-15 (Fig. 4 and Fig. S1, Supplementary Material) show a broad band around 3437 cm^{-1} (PCH) and 3426 cm^{-1} (SBA-15) with a shoulder at 3650 cm^{-1} (PCH) and 3630 cm^{-1} (SBA-15) due to O–H stretching vibrations of surface silanols and remaining physisorbed water, a peak at 1639 cm^{-1} (PCH) and 1630 cm^{-1} (SBA-15) related with the bending vibrations of adsorbed water, as well as the characteristic bands of the silica framework in the 1300–400 cm^{-1} range: a strong intensity band centred at 1085 cm^{-1} with a shoulder at 1220 cm^{-1} from asymmetric Si–O–Si stretching vibrations, a band near 800 cm^{-1} assigned to symmetric Si–O–Si stretching and a band at 465 cm^{-1} assigned to Si–O–Si bending modes [28,52–54]. The band in the 970–950 cm^{-1} range is assigned to the dangling ν(Si–O$_d$) due to Si–OH and Si–O$^-$ groups [28].

The APTES post-grafting is confirmed by the appearance of new peaks in the ranges of 2960–2850 and 1470–1385 cm^{-1} associated with C–H stretching and bending vibrations, respectively (APTES@PCH: 2920, 2850, 1472 and 1465 cm^{-1}; APTES@SBA-15: 2960, 2937, 2870, 1470, 1449, 1412 and 1385 cm^{-1}), and a weak and broad band around 1560 cm^{-1} due to N–H bending vibrations of primary amines (APTES@PCH: 1558 and 1541 cm^{-1}; APTES@SBA-15: 1559 and 1543 cm^{-1}) [22,50]. The bands related with N–H stretching vibrations around 3360 and 3290 cm^{-1} [22,50] could only be detected by high amplification of the OH stretching vibrations region. Furthermore, new weak bands in the ranges of 720–668 and 690–669 cm^{-1} can be noticed in the spectra of APTES@PCH and APTES@SBA-15, respectively, which are probably related with N–H bending modes, in agreement with literature [49,55]. The Si–CH$_2$–R and C–N stretching vibration bands, normally occurring in the ranges of 1250–1200 and 1200–1000 cm^{-1}, respectively, could not be detected due to their overlap with the strong intensity Si–O–Si stretching band [49,55]. The significant reduction of the OH stretching and bending vibration bands as well as of the band associated with Si–OH vibrations (970 cm^{-1}) confirms our proposed silane grafting mechanism, Scheme 1, catalysed by the adsorbed water, thus corroborating the results obtained by XPS (decrease in the oxygen surface content).

All the [M(acac)$_2$] based materials show similar differences in their FTIR spectra in comparison with the corresponding parent materials, although the differences are very small due to the low complex loadings. In the high energy region, there are changes in the C–H stretching vibrations range which are an indication of the presence of [M(acac)$_2$] [56]. In the 1700–1380 cm^{-1} range, new bands can be observed, with the most important one being the new band centred around 1645–1647 cm^{-1} for [M(acac)$_2$]APTES@PCH materials, 1641 cm^{-1} for [VO(acac)$_2$]APTES@SBA-15 and 1658 cm^{-1} for [Cu(acac)$_2$]APTES@SBA-15; in all cases a shoulder ~1620 or 1625 cm^{-1} for PCH and SBA-15 materials, respectively, can also be detected. These bands show different frequencies when compared to those of the free [M(acac)$_2$] complexes [56,57], which is an indication of a change in the coordination sphere of the complexes. Therefore, the new bands/shoulders can be assigned to vibrations associated with the new metal NO$_3$ coordination sphere, resulting from the complexes grafting through Schiff condensation between the NH$_2$-surface groups and the carbonyl group of the acac ligand, leading to the formation of a C=N bond. The same band patterns were also reported for [Cu(acac)$_2$] and [VO(acac)$_2$] complexes immobilised onto APTES modified clays [14,18]. In the former case, the optimised structure of the model molecule [Cu(acac)$_2$]-APTES was predicted at the DFT level and its IR spectrum was generated [18]; the selected IR vibration modes in the 1540–1660 cm^{-1} range (1541, 1566, 1567, 1634 and 1653 cm^{-1}) were in good agreement with those detected experimentally. These theoretical values can also be used in this work to prove the proposed grafting mechanism for the immobilisation of Cu(II) complex in PCH and SBA-15 (see new bands highlighted in Fig. 4 and Fig. S1, Supplementary Material). In this study, a similar procedure was applied to the model molecule [VO(acac)$_2$]-APTES. The most relevant band frequencies predicted in the 1350–1700 cm^{-1} range and the corresponding assignments to normal vibration modes of the chelate rings are depicted in Fig. 5 by vector displacement representation: (a) 1395 cm^{-1}, (b) 1418 cm^{-1}, (c) 1543 cm^{-1}, (d) 1545 cm^{-1}, (e) 1620 cm^{-1} and (f) 1634 cm^{-1}. There is a good agreement between the bands observed in the experimental spectra of [VO(acac)$_2$]-APTES based materials (Fig. 4 and Fig. S1, Supplementary Material) and the predicted theoretical wavenumbers (Fig. 5), which supports the same grafting mechanism for [VO(acac)$_2$] complex onto NH$_2$-functionalised PCH and SBA-15.

3.3. Catalytic studies

3.3.1. Epoxidation of geraniol

The catalytic performance of the [VO(acac)$_2$] based materials was evaluated in the geraniol epoxidation at room temperature, in CH$_2$Cl$_2$ using *t*-BuOOH as oxidant, and compared with those of the free complex and supports (Table 4).

To provide a full characterisation of the catalytic systems in terms of identification and quantification of all the reagents and products, studies in the homogeneous phase were firstly performed. The GC-FID chromatograms showed that the homogeneous phase reactions ended after half an hour and led to 100% geraniol conversion and 100% 2,3-epoxygeraniol yield. One of the reaction mixtures was fractionated by column chromatography and the isolated products were characterised by ^{1}H NMR [58] and GC–MS. The major product was 2,3-epoxygeraniol isolated in 92% yield. The ^{1}H NMR spectra of the total reaction mixtures under homogeneous conditions also showed 100% geraniol conversion, yielding 89% of 2,3-epoxygeraniol. In this context, the GC-FID results were in accordance with those obtained from ^{1}H NMR and 2,3-epoxygeraniol isolated yield and thus this technique could be used to determine substrate conversions, products selectivities and 2,3-epoxygeraniol yields for the heterogeneous phase reactions.

In the first cycle, both [VO(acac)$_2$] heterogeneous catalysts show moderate geraniol conversions but with high selectivities towards the 2,3-epoxygeraniol product (Table 4). The [VO(acac)$_2$]APTES@PCH material, compared to the SBA-15 one, presents slightly higher geraniol conversion and 2,3-epoxygeraniol yield, despite its lower V content. These facts seem to be related with the complex location within the supports: in [VO(acac)$_2$]APTES@PCH, the complex is localised in the external surface of the support; in contrast, in [VO(acac)$_2$]APTES@SBA-15, is mainly anchored in the material inner pores, which probably restrains the access of the substrate and oxidant to the catalytic active sites. Nevertheless, a slightly higher selectivity to 2,3-epoxygeraniol is achieved with the [VO(acac)$_2$]APTES@SBA-15 catalyst.

In all the heterogeneous reactions, a new peak with retention time close to geraniol was observed in the GC-FID chromatograms. Moreover, the ^{1}H NMR spectra of the corresponding reaction mixtures showed a doublet at δ(ppm) = 9.92, which confirmed the presence of geranial. Therefore, the small decrease in the 2,3-epoxygeraniol selectivity in heterogeneous systems is due to the formation of geranial as reaction product. The longer reaction times in the heterogeneous phase can justify the oxidation of geraniol to the aldehyde to some extent, but some of the geranial can also result from the catalytic activity of the supports themselves (see below).

Table 4
Epoxidation of geraniol, at room temperature, catalysed by [VO(acac)$_2$] in homogeneous and heterogeneous phases[a].

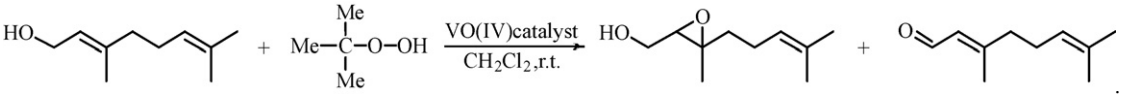

Sample	Run	t (h)	Conversion[b] (%)	S[c] (%)		2,3-EG Yield[d] (%)
				2,3-EG	Geranial	
PCH	1st	48	43	0	100	0
APTES@PCH	1st	48	7	0	100	0
[VO(acac)$_2$]APTES@PCH	1st	48	42	81	19	33
	2nd	48	40	73	27	24
	3rd	48	50	77	23	33
SBA-15	1st	48	7	0	100	0
APTES@SBA-15	1st	48	14	0	100	0
[VO(acac)$_2$]APTES@SBA-15	1st	48	34	88	12	29
	2nd	48	35	75	25	23
	3rd	48	32	88	12	27
[VO(acac)$_2$] (0.9%)[e]	1st	0.25	100	100	0	100
[VO(acac)$_2$] (1.4%)[f]	1st	0.25	100	100	0	100

[a] Reaction conditions: 1.00 mmol of geraniol, 0.50 mmol of chlorobenzene (internal standard), 0.10 g of heterogeneous material, 1.50 mmol of t-BuOOH; solvent: CH_2Cl_2.
[b] Based on geraniol consumption.
[c] Products selectivity: 2,3-EG = 2,3-epoxygeraniol.
[d] Determined by GC-FID using chlorobenzene as internal standard and isolated 2,3-EG product.
[e] Homogeneous phase reaction using the same V loading as [VO(acac)$_2$]APTES@PCH.
[f] Homogeneous phase reaction using the same V loading as [VO(acac)$_2$]APTES@SBA-15.

Recycling experiments were performed for further two cycles. The V bulk contents determined after the three cycles, 80 and 130 μmol g^{-1} for [VO(acac)$_2$]APTES@PCH and [VO(acac)$_2$]APTES@SBA-15, respectively, correspond to leaching percentages of only 7% and 5%. These heterogeneous catalysts are stable and maintain, in average, their catalytic activities upon reuse (Table 4).

The original and APTES-functionalised supports, with the exception of unmodified PCH, present low catalytic activities and 100% selectivities towards geranial; no formation of the desired product, 2,3-epoxygeraniol, is observed (Table 4). The catalytic activity of PCH can be justified based on its structural composition. It has been reported that K10 montmorillonite clay, which also presents an aluminosilicate framework, is catalytically active in the oxidation of alcohols to carbonyl products with t-BuOOH, due to the presence of reactive aluminium atoms [59]; nonetheless, the APTES functionalisation of PCH results in a significantly lower catalytic activity, indicating that APTES blocks the active sites of the PCH.

Finally, the reaction times are longer than those of the homogeneous reactions due to diffusion constraints imposed on substrates and reactants by the silica porosity [14,15].

3.3.2. Aziridination of styrene

The catalytic activity of [Cu(acac)$_2$] complex in homogeneous and heterogeneous phases was evaluated in the styrene aziridination in CH_3CN, at room temperature, using PhI = NTs as nitrogen source (Table 5). All the reactions were monitored by GC-FID and those using the supports, 1.2% [Cu(acac)$_2$] complex and immobilised [Cu(acac)$_2$] catalysts after three catalytic runs were also analysed by ^{1}H NMR.

The homogeneous reaction performed with 1.2% catalyst relatively to styrene was fractioned by column chromatography. Two different fractions were obtained and identified by ^{1}H NMR, one containing iodobenzene and the other a mixture of aziridine and p-toluenesulfonamide in a 76:24 ratio. The sulphonamide was removed by precipitation from CH_2Cl_2:petroleum ether and subsequent filtration, affording the pure aziridine in 75% yield. The ^{1}H NMR spectrum of the corresponding total reaction mixture showed that, besides the aziridine, the p-toluenesulfonamide was also formed resulting from the competitive degradation of the nitrogen source. The PhI = NTs decomposition to p-toluenesulfonamide was observed in the same extension even in dry or inert conditions. The aziridine yield was determined from the ^{1}H NMR total reaction spectrum, based on the proton integrals of aziridine and p-toluenesulfonamide peaks, being 72%, in accordance with the isolated yield. In literature it has been reported the competitive decomposition of PhI = NTs to iodobenzene and sulphonamide occurring simultaneously with the aziridination reaction, corroborating our results [3,44]. Taylor et al. investigated the effect of the nitrene donor on the styrene aziridination using PhI = NTs or [N-(p-nitrophenylsulfonyl)imino]phenyliodinane as nitrene donors and copper(II) triflate or copper-exchanged zeolite Y as catalysts [44]. They observed that the addition of the breakdown products of the nitrogen source, iodobenzene and sulfonamide, in the beginning of the reactions, led to a decrease both in the reaction rates and total aziridine yields, being more marked in the heterogeneous phase probably due to pore diffusion constraints.

In the first catalytic cycle of heterogeneous reactions the catalysts present moderate activities, with [Cu(acac)$_2$]APTES@SBA-15 showing slightly higher styrene conversion than the PCH counterpart. Both catalysts present lower substrate conversions and higher reaction times than the corresponding homogeneous catalyst, owing to inherent diffusion constraints imposed on substrates and reactants by the porous matrix, since the nitrogen source is a solid with limited solubility in CH_3CN, with its solubilisation being controlled by its consumption rate [3].

The catalysts reusability was tested for other two cycles and a decrease in the styrene conversion could be observed from cycle to cycle. To confirm that the styrene conversion corresponds to the formation of the aziridine product after three catalytic cycles, the crude mixtures were analysed by ^{1}H NMR. The aziridine yields were 28% and 35% for [Cu(acac)$_2$]APTES@PCH and [Cu(acac)$_2$]APTES@SBA-15, respectively, in agreement with the $\%C_{styrene}$ values, indicating that all the reacted styrene substrate affords the desired aziridine. However, the yields of p-toluenesulfonamide were higher than in the homogeneous phase,

Table 5
Aziridination of styrene, at room temperature, catalysed by [Cu(acac)$_2$] in homogeneous and heterogeneous phases[a].

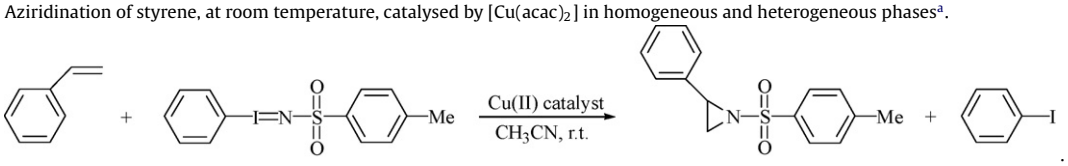

Sample	Run	t[b] (h)	Conversion[c] (%)	Yield[d] (%)
PCH	1st	24	21	0
APTES@PCH	1st	24	12	0
[Cu(acac)$_2$]APTES@PCH	1st	24	55	ND
	2nd	24	40	ND
	3rd	24	29	28
SBA-15	1st	24	38	0
APTES@SBA-15	1st	24	17	0
[Cu(acac)$_2$]APTES@SBA-15	1st	24	59	ND
	2nd	24	41	ND
	3rd	24	33	35
[Cu(acac)$_2$] (0.4%)[e]	1st	1	77	ND
[Cu(acac)$_2$] (1.2%)[f]	1st	1	72	72

[a] Reaction conditions: 1.22 mmol of styrene, 1.22 mmol of chlorobenzene (internal standard), 0.10 g of heterogeneous material, 0.244 mmol of PhI = NTs; solvent: CH_3CN.
[b] Time needed for total consumption of PhI = NTs.
[c] Styrene conversion, corrected for limiting reagent (PhI = NTs).
[d] Aziridine yield determined by ^{1}H NMR.
[e] Homogeneous phase reaction using the same Cu content as [Cu(acac)$_2$]APTES@PCH.
[f] Homogeneous phase reaction using the same Cu content as [Cu(acac)$_2$]APTES@SBA-15.

probably due to the slower kinetics of the reactions which induces higher PhI = NTs decomposition. The Cu bulk contents after three catalytic runs, 28 and 27 μmol g^{-1} for [Cu(acac)$_2$]APTES@PCH and [Cu(acac)$_2$]APTES@SBA-15, respectively, lead to complex leaching percentages of 40% and 81%, respectively. Even though [Cu(acac)$_2$]APTES@SBA-15 presents higher initial Cu loading and shows slightly higher substrate conversion and aziridine yield than the PCH counterpart, the latter is more stable upon reuse for three cycles. On the basis of these results, it can be concluded that the grafting method is not very robust under the aziridination catalytic conditions.

In terms of the intrinsic catalytic activity of the supports, the parent materials lead to some substrate consumption which decreases upon their functionalisation with APTES. Nevertheless, for both parent and functionalised materials, the ^{1}H NMR spectra of the reaction mixtures revealed the absence of the aziridine product, suggesting that the styrene decrease can be due to its adsorption inside the pores of the materials.

4. Concluding remarks

The complexes [VO(acac)$_2$] and [Cu(acac)$_2$] were covalently immobilised onto APTES-functionalised PCH and SBA-15 with anchoring efficiencies of 57%, 31%, 91% and 95% for [VO(acac)$_2$]APTES@PCH, [Cu(acac)$_2$]APTES@PCH, [VO(acac)$_2$]APTES@SBA-15 and [Cu(acac)$_2$]APTES@SBA-15, respectively. In [VO(acac)$_2$]APTES@PCH, [Cu(acac)$_2$]APTES@PCH and [Cu(acac)$_2$]APTES@SBA-15 the complexes were mostly immobilised on the supports external surface, whereas in [VO(acac)$_2$]APTES@SBA-15 the complex was mainly anchored in the inner pores. The experimental FTIR spectra combined with the predicted theoretical IR spectra of model molecules [M(acac)$_2$]-APTES confirmed the complexes grafting mechanism through Schiff condensation between the free amine groups of the supports surface and the C=O groups of the complexes, leading to a NO_3 coordination sphere for the metal centre.

The [VO(acac)$_2$] based materials acted as active catalysts in the epoxidation of geraniol using t-BuOOH, showing moderate geraniol conversions and high selectivity towards 2,3-epoxygeraniol. Although [VO(acac)$_2$]APTES@PCH presented a lower V content than [VO(acac)$_2$]APTES@SBA-15, it led to slightly higher geraniol conversion and epoxide yield, probably due to the more external location of the complex. However, a slightly higher selectivity to 2,3-epoxygeraniol was achieved with [VO(acac)$_2$]APTES@SBA-15. Both catalysts were highly stable upon reuse for two cycles and maintained their catalytic activities, without almost no leaching.

The [Cu(acac)$_2$] based materials presented moderate catalytic activities in the aziridination of styrene with PhI = NTs. [Cu(acac)$_2$]APTES@SBA-15 led to a slightly higher styrene conversion than the PCH counterpart. However, upon reuse for further two cycles, both catalysts showed a decrease in the styrene conversions and high complex leaching %s highlighting that, in this particular case, the complex grafting methodology was not robust under the catalytic reaction conditions.

Finally, it is noteworthy that, although higher [M(acac)$_2$] immobilisation efficiencies were obtained for SBA-15 materials, the PCH based catalysts were more stable in epoxidation and aziridination reactions. Therefore, the support itself and ultimately the catalyst loading and complex location within the support have important contributions in the catalytic performance of the immobilised catalysts.

Acknowledgments

The authors are indebted to Dr. Carlos Sá (CEMUP) for assistance with XPS analysis. This work was funded by Fundação para a Ciência e a Tecnologia and FEDER, through project ref. PPCDT/CTM/56192/2004. CP thanks FCT for a PhD fellowship.

Appendix A. Supplementary data

Supplementary data associated with this article can be found, in the online version, at doi:10.1016/j.molcata.2009.07.004.

References

[1] C. Bolm, Coord. Chem. Rev. 237 (2003) 245–256.

[2] Q.-H. Xia, H.-Q. Ge, C.-P. Ye, Z.-M. Liu, K.-X. Su, Chem. Rev. 105 (2005) 1603–1662.
[3] D.A. Evans, M.M. Faul, M.T. Bilodeau, J. Org. Chem. 56 (1991) 6744–6746.
[4] P. Müller, C. Fruit, Chem. Rev. 103 (2003) 2905–2919.
[5] A. Lattanzi, N.E. Leadbeater, Org. Lett. 4 (2002) 1519–1521.
[6] M.L. Kantam, B. Kavita, V. Neeraja, Y. Haritha, M.K. Chaudhuri, S.K. Dehury, Tetrahedron Lett. 44 (2003) 9029–9032.
[7] (a) K.B. Sharpless, R.C. Michaelson, J. Am. Chem. Soc. 95 (1973) 6136–6137;
(b) B.E. Rossiter, T.R. Verhoeven, K.B. Sharpless, Tetrahedron Lett. 20 (1979) 4733–4736;
(c) T. Itoh, K. Jitsukawa, K. Kaneda, S. Teranishi, J. Am. Chem. Soc. 101 (1979) 159–169.
[8] V. Conte, F. Di Furia, G. Licini, Appl. Catal. A: Gen. 157 (1997) 335–361.
[9] A.G.J. Ligtenbarg, R. Hage, B.L. Feringa, Coord. Chem. Rev. 237 (2003) 89–101.
[10] M.H. Valkenberg, W.F. Hölderich, Catal. Rev. 44 (2002) 321–374.
[11] D.E. De Vos, M. Dams, B.F. Sels, P.A. Jacobs, Chem. Rev. 102 (2002) 3615–3640.
[12] B.M.L. Dioos, I.F.J. Vankelecom, P.A. Jacobs, Adv. Synth. Catal. 348 (2006) 1413–1446.
[13] A. Corma, H. Garcia, Adv. Synth. Catal. 348 (2006) 1391–1412.
[14] C. Pereira, A.R. Silva, A.P. Carvalho, J. Pires, C. Freire, J. Mol. Catal. A: Chem. 283 (2008) 5–14.
[15] B. Jarrais, A.R. Silva, C. Freire, Eur. J. Inorg. Chem. (2005) 4582–4589.
[16] A.R. Silva, J.L. Figueiredo, C. Freire, B. de Castro, Catal. Today 102–103 (2005) 154–159.
[17] A.R. Silva, K. Wilson, A.C. Whitwood, J.H. Clark, C. Freire, Eur. J. Inorg. Chem. (2006) 1275–1283.
[18] C. Pereira, S. Patrício, A.R. Silva, A.L. Magalhães, A.P. Carvalho, J. Pires, C. Freire, J. Colloid Interface Sci. 316 (2007) 570–579.
[19] A.R. Silva, M. Martins, M.M.A. Freitas, J.L. Figueiredo, C. Freire, B. de Castro, Eur. J. Inorg. Chem. (2004) 2027–2035.
[20] M. Baltes, O. Collart, P. Van der Voort, E.F. Vansant, Langmuir 15 (1999) 5841–5845.
[21] A.-M. Hanu, S. Liu, V. Meynen, P. Cool, E. Popovici, E.F. Vansant, Micropor. Mesopor. Mater. 95 (2006) 31–38.
[22] S. Shylesh, A.P. Singh, J. Catal. 244 (2006) 52–64.
[23] P. Kuśtrowski, L. Chmielarz, R. Dziembaj, P. Cool, E.F. Vansant, J. Phys. Chem. B 109 (2005) 11552–11558.
[24] A. Galarneau, A. Barodawalla, T.J. Pinnavaia, Nature 374 (1995) 529–531.
[25] J. Pires, A.C. Araújo, A.P. Carvalho, M.L. Pinto, J.M. González-Calbet, J. Ramírez-Castellanos, Micropor. Mesopor. Mater. 73 (2004) 175–180.
[26] M. Benjelloun, P. Cool, T. Linssen, E.F. Vansant, Micropor. Mesopor. Mater. 49 (2001) 83–94.
[27] M. Polverejan, T.R. Pauly, T.J. Pinnavaia, Chem. Mater. 12 (2000) 2698–2704.
[28] J. Pires, M. Pinto, J. Estella, J. Echeverría, J. Colloid Interface Sci. 317 (2008) 206–213.
[29] M.L. Pinto, J. Pires, J. Rocha, J. Phys. Chem. C 112 (2008) 14394–14402.
[30] M. Choi, F. Kleitz, D. Liu, H. Yoon Lee, W.S. Ahn, R. Ryoo, J. Am. Chem. Soc. 127 (2005) 1924–1932.
[31] D. Zhao, J. Feng, Q. Huo, N. Melosh, G.H. Fredrickson, B.F. Chmelka, G.D. Stucky, Science 279 (1998) 548–552.
[32] K. Cassiers, T. Linssen, M. Mathieu, M. Benjelloun, K. Schrijnemakers, P. Van Der Voort, P. Cool, E.F. Vansant, Chem. Mater. 14 (2002) 2317–2324.
[33] A. Taguchi, F. Schüth, Micropor. Mesopor. Mater. 77 (2005) 1–45.
[34] F. Chiker, F. Launay, J.P. Nogier, J.L. Bonardet, Green Chem. 5 (2003) 318–322.
[35] A. Sakthivel, J. Zhao, F.E. Kühn, Micropor. Mesopor. Mater. 86 (2005) 341–348.
[36] F. Rouquerol, J. Rouquerol, K. Sing, Adsorption by Powders and Porous Solids, Academic Press, San Diego, 1999.
[37] A.D. Becke, J. Chem. Phys. 98 (1993) 5648–5652.
[38] C. Lee, W. Yang, R.G. Parr, Phys. Rev. B 37 (1988) 785–789.
[39] P.J. Hay, W.R. Wadt, J. Chem. Phys. 82 (1985) 270–283.
[40] J.P. Merrick, D. Moran, L. Radom, J. Phys. Chem. A 111 (2007) 11683–11700.
[41] Gaussian 03, Revision C.02, M.J. Frisch, G.W. Trucks, H.B. Schlegel, G.E. Scuseria, M.A. Robb, J.R. Cheeseman, J.A. Montgomery, Jr., T. Vreven, K.N. Kudin, J.C. Burant, J.M. Millam, S.S. Iyengar, J. Tomasi, V. Barone, B. Mennucci, M. Cossi, G. Scalmani, N. Rega, G.A. Petersson, H. Nakatsuji, M. Hada, M. Ehara, K. Toyota, R. Fukuda, J. Hasegawa, M. Ishida, T. Nakajima, Y. Honda, O. Kitao, H. Nakai, M. Klene, X. Li, J.E. Knox, H.P. Hratchian, J.B. Cross, V. Bakken, C. Adamo, J. Jaramillo, R. Gomperts, R.E. Stratmann, O. Yazyev, A.J. Austin, R. Cammi, C. Pomelli, J.W. Ochterski, P.Y. Ayala, K. Morokuma, G.A. Voth, P. Salvador, J.J. Dannenberg, V.G. Zakrzewski, S. Dapprich, A.D. Daniels, M.C. Strain, O. Farkas, D.K. Malick, A.D. Rabuck, K. Raghavachari, J.B. Foresman, J.V. Ortiz, Q. Cui, A.G. Baboul, S. Clifford, J. Cioslowski, B.B. Stefanov, G. Liu, A. Liashenko, P. Piskorz, I. Komaromi, R.L. Martin, D.J. Fox, T. Keith, M.A. Al-Laham, C.Y. Peng, A. Nanayakkara, M. Challacombe, P.M.W. Gill, B. Johnson, W. Chen, M.W. Wong, C. Gonzalez, J.A. Pople, Gaussian, Inc., Wallingford CT, 2004.
[42] GaussView, Version 4.1, R. Dennington II, T. Keith, J. Millam, Semichem, Inc., Shawnee Mission, KS, 2007.
[43] K. Nakamoto, Y. Morimoto, A.E. Martell, J. Am. Chem. Soc. 83 (1961) 4533–4536.
[44] S. Taylor, J. Gullick, P. McMorn, D. Bethell, P.C.B. Page, F.E. Hancock, F. King, G.J. Hutchings, J. Chem. Soc., Perkin Trans. 2 (2001) 1714–1723.
[45] L. Wei, T. Tang, B. Huang, Micropor. Mesopor. Mater. 67 (2004) 175–179.
[46] R. Ryoo, C.H. Ko, M. Kruk, V. Antochshuk, M. Jaroniec, J. Phys. Chem. B 104 (2000) 11465–11471.
[47] W.W. Lukens Jr., P. Schmidt-Winkel, D. Zhao, J. Feng, G.D. Stucky, Langmuir 15 (1999) 5403–5409.
[48] M.B. de Carvalho, J. Pires, A.P. Carvalho, Micropor. Mater. 6 (1996) 65–77.
[49] A.S.M. Chong, X.S. Zhao, J. Phys. Chem. B 107 (2003) 12650–12657.
[50] S.-W. Song, K. Hidajat, S. Kawi, Langmuir 21 (2005) 9568–9575.
[51] K.M.R. Kallury, P.M. MacDonald, M. Thompson, Langmuir 10 (1994) 492–499.
[52] D. Pérez-Quintanilla, I. del Hierro, M. Fajardo, I. Sierra, J. Mater. Chem. 16 (2006) 1757–1764.
[53] P. Shah, A.V. Ramaswamy, K. Lazar, V. Ramaswamy, Appl. Catal. A: Gen. 273 (2004) 239–248.
[54] Q. Cheng, V. Pavlinek, A. Lengalova, C. Li, Y. He, P. Saha, Micropor. Mesopor. Mater. 93 (2006) 263–269.
[55] X. Wang, K.S.K. Lin, J.C.C. Chan, S. Cheng, J. Phys. Chem. B 109 (2005) 1763–1769.
[56] K. Nakamoto, Infrared and Raman Spectra of Inorganic and Coordination Compounds, John Wiley & Sons, Inc., New York, 1997.
[57] P. Van der Voort, I.V. Babitch, P.J. Grobet, A.A. Verberckmoes, E.F. Vansant, J. Chem. Soc. Faraday Trans. 92 (1996) 3635–3642.
[58] R.R.L. Martins, M.G.P.M.S. Neves, A.J.D. Silvestre, M.M.Q. Simões, A.M.S. Silva, A.C. Tomé, J.A.S. Cavaleiro, P. Tagliatesta, C. Cresini, J. Mol. Catal. A: Chem. 172 (2001) 33–42.
[59] L. Palombi, F. Bonadies, A. Scettri, J. Mol. Catal. A: Chem. 140 (1999) 47–53.